Mechanism Analysis of Additional Damping Control Strategies for the High-frequency Resonance of MMC Connected to AC Grid

Yanqi Hou, *Student Member*, *IEEE*, Chongru Liu, *Senior Member*, *IEEE*, Yu Wang, and Wei Kong

***Abstract*—High-frequency resonance can occur when a modular multilevel converter (MMC) is inserted into an AC grid. Additional damping control is a relatively low-cost resonance suppression strategy compared to passive damping strategies. This paper analyzes the influences of a feed-forward voltage filter and feedback current filter for the inner controller for the high-frequency impedance characteristics of the MMC based on a model. Moreover, the mechanism, influencing factors, and limitations of the existing strategy including an additional low-pass filter in the voltage feed-forward stage are investigated. Secondly, a resonance suppression strategy for the inclusion of additional cascaded notch filters in the voltage feed-forward stage is proposed, and its parameter design method and applicable scenarios are analyzed. In addition, this paper analyzes the effects of the inclusion of an additional control in other stages for the inner controller of the MMC. Finally, the correctness of the theoretical analysis and the proposed strategy is verified based on the simulation of an actual project on PSCAD/EMTDC.**

***Index Terms*—Additional damping control strategy, additional cascaded notch filters, additional low-pass filter, modular multilevel converter (MMC), high-frequency resonance.**

I. INTRODUCTION

FLEXIBLE high-voltage direct-current (HVDC) transmission technology has developed rapidly since its initial proposal. Particularly, modular multilevel converter (MMC)-based HVDC transmission technology, which has advantages in terms of its harmonic level, independent control, and many other aspects as compared to line-commutated converter (LCC)-based HVDC transmission technology, is widely used in large-capacity long-distance transmission, offshore wind energy transmission, and many other scenarios [1]–[3].

With the maturity of MMC-HVDC transmission technology and the growth of power demands, the number of submodules (SMs), the capacity, and the voltage of MMC-HVDC projects have increased. This makes the control and protection system of MMC inconvenient to integrate and the signal transmission process complex, resulting in long link delay that is difficult to reduce, which ultimately affects the stability between the DC and AC systems and easily causes high-frequency resonance [4]–[6]. In recent years, many high-frequency resonance phenomena caused by MMC have occurred, which has become a problem that cannot be ignored [7]–[9].

At present, the research on an additional damping control strategy for the high-frequency resonance of a MMC connected to the AC grid is relatively immature and still in the exploration stage. However, after further research, the effect of the voltage feed-forward stage of the inner controller on high-frequency resonance has been recognized, and a few effective additional control strategies have been proposed. [10]–[12]. Reference [13] discussed the resonance which occurred in China's Luxi back-to-back HVDC project and proposed a strategy of adding a low-pass filter in the voltage feed-forward stage, which, at present, is a typical additional control strategy for high-frequency resonance. Reference [14] proposed a strategy of a nonlinear filter for the feed-forward voltage to solve the high-frequency resonance of China's Chongqing-Hubei back-to-back HVDC project. Its function is equivalent to retaining only the fundamental frequency component of the feed-forward voltage, so it can more significantly compensate negative damping. Reference [15] proposed to add the processed feed-forward voltage to the reference current of the inner controller, which has the same effect as the strategy of adding a low-pass filter to the voltage feed-forward stage. Reference [16] proposed a strategy of adding a single band-stop filter to the voltage feed-forward stage to realize phase compensation at a specific frequency and improved the compensation effect by increasing the damping ratio.

However, the existing additional control strategies for high-frequency resonance exhibit limitations in both simulation and practice [15]. For example, during the test of the Chongqing-Hubei project, a high-frequency resonance of about 695 Hz occurred in the Chongqing-side system after the use of the first-order low-pass filter. To date, there have only been a few studies on the additional damping control strategy for high-frequency resonance, and there has been no theoretical analysis of its reasons for failure.

In this paper, the influence of each stage for the inner controller of the MMC on its high-frequency impedance is

Manuscript received November 24, 2020; revised February 17, 2021; accepted May 12, 2021. Date of online publication December 30, 2021; date of current version October 24, 2022. This work was supported in part by Science and Technology Project of State Grid Corporation of China, "Research on Harmonic Oscillation Problems and Suppression Strategies of Flexible DC Connected to AC Grid", (No. SGTYHT/17-JS-199).

Y. Q. Hou and C. R. Liu (corresponding author, email: chongru.liu@ncepu.edu.cn) are with the State Key Laboratory for Alternate Electrical Power System with Renewable Energy Sources, North China Electric Power University, Beijing 102206, China.

Y. Wang is with State Grid Economic and Technological Research Institute Co. Ltd., Beijing 102209, China.

W. Kong is with State Grid Corporation of China, Beijing 100031, China.

DOI: 10.17775/CSEEJPES.2020.06340

analyzed and the mechanism of typical additional damping control is studied by using the impedance analysis method. Then, considering the actual impedance characteristics of the AC system, an additional strategy based on cascaded notch filters is proposed, and its parameters are designed. The proposed strategy can realize local compensation for the impedance of MMC at multiple frequencies with a small damping ratio, thereby reducing its impact on the performance of the inner controller. In addition, several additional controls for other structures are proposed and analyzed. The limitations and applicable scenarios of these strategies are determined via theoretical analysis, and the correctness of the proposed method is verified by simulations conducted in PSCAD/EMTDC.

II. Impedance Characteristics Analysis

A. Impedance Characteristics of the AC System

Due to the influence of the distributed parameters of long AC overhead lines, the high-frequency impedance characteristics of the AC system from the PCC change with the frequency, which is an important reason why high-frequency resonance is difficult to suppress.

In this paper, a detailed simulation model of the AC system is established in PSCAD/EMTDC, according to the structure of the Chongqing-side AC system of the northern route of the Chongqing-Hubei project. This model contains three adjacent buses including frequency-dependent overhead lines, series compensation, equivalent AC sources and so on. As shown in Fig. 1, the magnitude and phase of the AC system impedance at each frequency are calculated by injecting the harmonic current of the corresponding frequency into the AC system from PCC and reading its harmonic voltage.

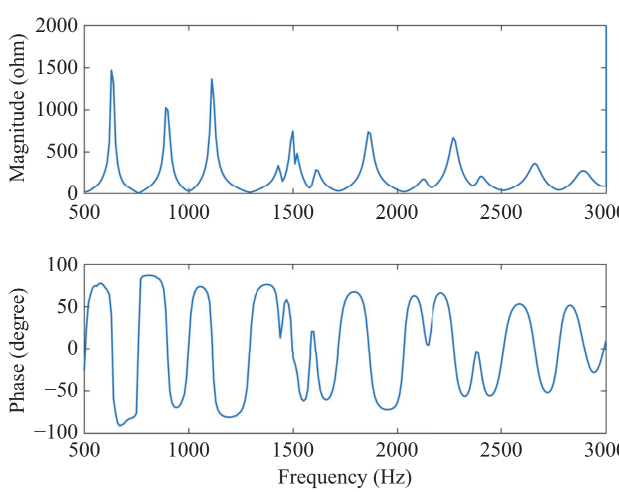

Fig. 1. Impedance-frequency characteristics of the AC system.

B. Impedance Characteristics of the MMC

The simulation model of the DC system is established based on the DC system of the northern route of the Chongqing-Hubei project; the parameters are listed in Table I.

In the high-frequency range, the influence of the outer controller, phase-locked loop (PLL), and current cross-forward terms on the impedance characteristics of the MMC can be ignored, and a simplified control block diagram, which is used to analyze high-frequency impedance characteristics of the MMC, is illustrated in Fig. 2 [17].

TABLE I
Parameters of the DC System

Parameter	Value
Rated AC voltage (kV)	525
AC frequency (Hz)	50
MMC transformer ratio (kV/kV)	525/437
Transformer capacity (single-phase) (MVA)	375
Transformer leakage reactance (p.u.)	0.14
Arm inductance L_{ARM} (H)	0.14
Rated DC voltage (kV)	± 420
Rated active power (MW)	2 × 1250
Rated reactive power (MVAr)	0
Inner controller proportional coefficient k_{p}	1
Inner controller integral coefficient k_{i}	30
Solution time step (μs)	50
Overall link delay T_{d} (μs)	500

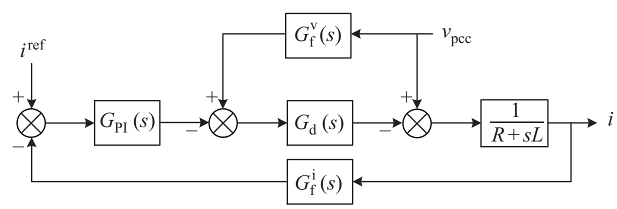

Fig. 2. MMC simplified control block diagram.

Where $G_{\mathrm{PI}}(s)=k_{\mathrm{p}}+k_{\mathrm{i}}/s$, $G_{\mathrm{f}}^{\mathrm{v}}(s)$ and $G_{\mathrm{f}}^{\mathrm{i}}(s)$ are the filters of the feed-forward voltage and feedback current, respectively, $G_{\mathrm{d}}(s)$ is the delay function, and R and L are the equivalent resistance and equivalent inductance, respectively, where $L=L_{\mathrm{T}}+L_{\mathrm{ARM}}/2$. According to the parameters in Table I, $L=0.18$ H.

The model of the high-frequency impedance of the MMC is obtained by deducing the transfer function of the control loop shown in Fig. 2.

$$Z_{\mathrm{M}}(s)=\frac{R+sL+G_{\mathrm{f}}^{\mathrm{i}}(s)G_{\mathrm{d}}(s)(k_{\mathrm{p}}+k_{\mathrm{i}}/s)}{1-G_{\mathrm{f}}^{\mathrm{v}}(s)G_{\mathrm{d}}(s)} \tag{1}$$

1) PI Control

The parameters of the PI control affect system stability. The response speed of the inner controller is fast and the time constant of its integrator is usually at the level of milliseconds. However, the magnitude of the integrator is small at high frequency (>550 Hz), which is smaller than k_{p}, and decreases with the increase of frequency. Therefore, in the high-frequency range, the magnitude of $G_{\mathrm{PI}}(s)$ is approximately equal to k_{p} and the phase of $G_{\mathrm{PI}}(s)$ is approximately equal to 0.

2) Delay Function

$G_{\mathrm{d}}(s)$ can be expressed as (2).

$$G_{\mathrm{d}}(s)=e^{-sT_{\mathrm{d}}}=\cos(2\pi T_{\mathrm{d}}f)-j\sin(2\pi T_{\mathrm{d}}f) \tag{2}$$

Its magnitude is equal to 1 and the phase is equal to $-2\pi T_{\mathrm{d}}f$. The phase changes periodically with the frequency at a period of $1/T_{\mathrm{d}}$ when it is converted to the range of $\pm180°$.

When $G_f^v(s) = 1$, the magnitude and phase of the denominator of (1) changes periodically with the frequency due to the phase-shifting effect of $G_d(s)$, where the magnitude is equal to $2|\sin(2\pi T_d f)|$ and the phase is equal to $\pi(1/2 - T_d f)$. At the frequency $f_c = 1/T_d$, the magnitude is 0, and the phase changes from $-90°$ to $90°$, which will lead to a magnitude spike and phase jump of $Z_M(s)$.

3) R and L

R and L are main circuit parameters of MMC, where R is usually small enough to be ignored in the high-frequency range.

The effect of "sL" in (1) is equivalent to a differential, the phase of which is constantly 90°, and the magnitude increases linearly with the frequency. In the high-frequency range, the magnitude of "sL" is much larger than that of $G_{PI}(s)$.

4) Filters

The filter cannot lead to a large gain of magnitude. In the high-frequency range, the magnitude of "sL" is the largest among all terms in the numerator of (1), so the characteristics of the numerator is similar to that of "sL." In other words, the current filter has little effect on the high-frequency impedance characteristics of the MMC, and the voltage filter should be considered in the study of additional damping control.

Figure 3 presents the Bode plot of the impedance model of the MMC under the parameters listed in Table I when $G_f^v(s)$ and $G_f^i(s)$ are equal to 1. Compared with the Bode plot of the simplified impedance model, whose numerator is simplified as "sL," they are basically the same in the high-frequency range, only slightly different when the frequency is small. This shows that the above conclusions are correct. Therefore, in the high-frequency range, the phase of the numerator of (1) is approximately constant and the phase of $Z_M(s)$ primarily depends on the denominator of (1). When the phase of the denominator is less than 0, the MMC exhibits negative damping. Therefore, the negative damping of MMC is in the frequency range of roughly $[1/(2T_d), 1/T_d]$ Hz. In order to facilitate the analysis, the next section investigates the phase compensation mechanism of the additional damping control strategy based on the characteristics of the denominator of (1).

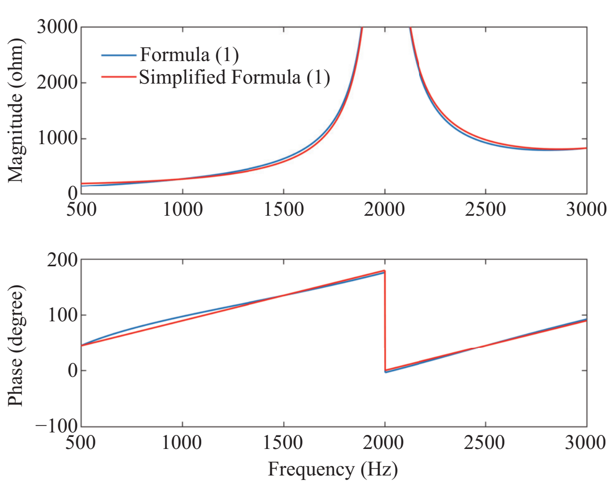

Fig. 3. Bode plot of the MMC impedance model.

Considering the AC system, the stability condition of the interconnected system is: at the intersection of the magnitude-frequency curves of $Z_M(s)$ and $Z_{AC}(s)$, the phase deviation of $Z_M(s)$ and $Z_{AC}(s)$ is not more than 180°, as shown in Fig. 4. Therefore, with the increase of T_d, the negative damping of MMC at the same frequency increases, and the risk of resonance increases.

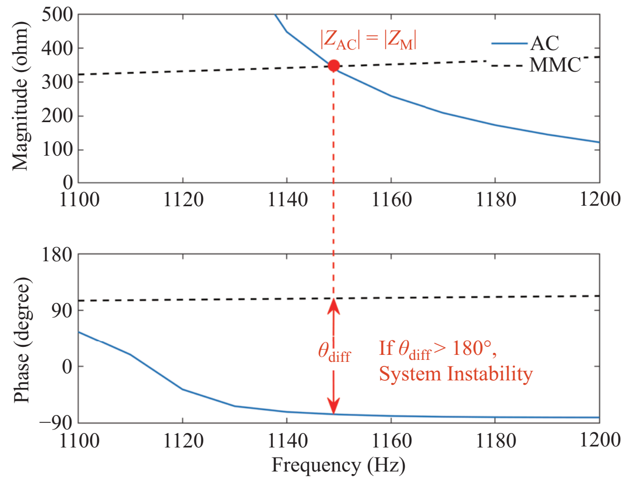

Fig. 4. System instability condition.

III. Study on Additional Damping Control

A. Additional Feed-forward Voltage Low-pass Filter

Equation (3) is the transfer function of the first-order low-pass filter, which is a typical method to suppress the high-frequency resonance of the MMC-HVDC system.

$$G_f^v(s) = \frac{1}{1 + sT_m} \tag{3}$$

where T_m is the time constant of the filter, and the corresponding cut-off frequency $f_m = 1/(2\pi T_m)$.

In the high-frequency range, the characteristic of the magnitude of the low-pass filter function being approximately 0 causes the phase of the denominator of (1) to be close to 0, thereby achieving the purpose of improving damping. The denominator of (1) after adding a low-pass filter can be expressed as (4).

$$1 - G_f^v(s)G_d(s) = 1 - |G_f^v(s)|\angle(\theta_f + \theta_d) \tag{4}$$

where θ_f and θ_d are the phases of the low-pass filter and delay function, respectively.

With the increase of frequency, θ_f decreases from 0 to $-90°$, and θ_d changes periodically between $\pm 180°$. Therefore, when $0 < \theta_f + \theta_d < 180°$, the phase of (4) is less than 0, indicating that the MMC still exhibits negative damping in some frequency ranges after the addition of a low-pass filter.

With the decrease of f_m, the speed at which θ_f changes with the frequency increases, causing the frequency range of the negative damping of the MMC to move toward a lower frequency, and the resonance frequency of the system may also shift accordingly. However, when f_m decreases, the speed at which $|G_f^v(s)|$ decreases with the increase of the frequency also increases, leading to the weakened negative damping of the MMC. Therefore, the phase margin can be improved by reducing the cut-off frequency of the first-order low-pass filter, but the response of the controller will be greatly affected. Fig. 5 presents the Bode plot of (4) with different values of T_{m}.

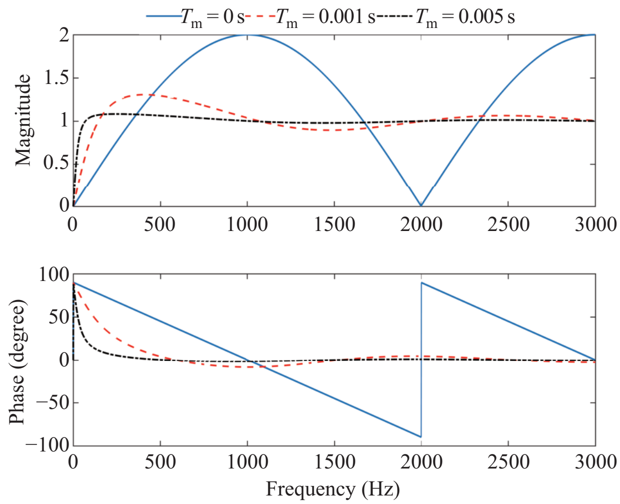

Fig. 5. Bode plot of the denominator of (1) with different values of T_{m}.

The high-order low-pass filter has the same limitations as the first-order low-pass filter, and the phase change of the former has a larger range and faster speed, which causes the frequency range of negative damping to be lower.

$$G_{\mathrm{f}}^{\mathrm{v}}(s) = \frac{\omega_{\mathrm{m}}^2}{s^2 + \xi\omega_{\mathrm{m}}s + \omega_{\mathrm{m}}^2} \tag{5}$$

Using the second-order low-pass filter as an example, the transfer function is shown in (5), where $\xi = 1.73$, $f_{\mathrm{m}} =$ 500 Hz. Fig. 6 presents the Bode plot of (4) with the same value of f_{m} and considering different orders.

Therefore, increasing the order of the low-pass filter has a limited effect on improving the phase compensation. The compensation effect of the low-pass filter can only be improved by reducing the cut-off frequency and sacrificing the performance of the control system of the MMC.

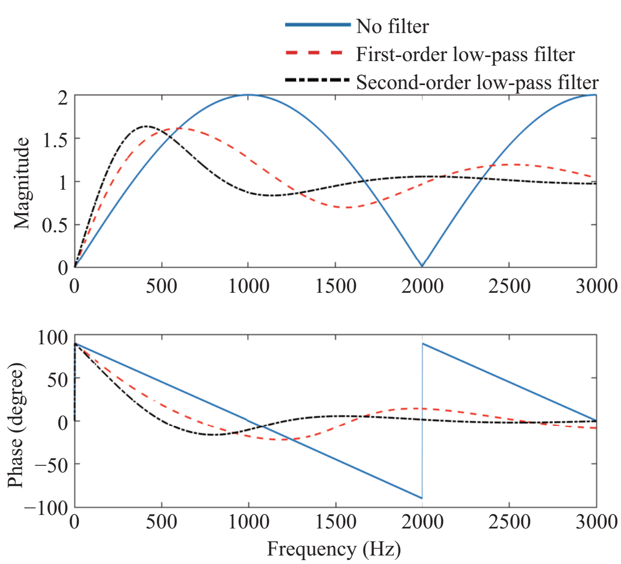

Fig. 6. Bode plot of the denominator of (1) with different orders ($f_{\mathrm{m}} =$ 500 Hz).

B. Additional Feed-forward Voltage Cascaded Notch Filters

1) Mechanism analysis

Similar to the mechanism of the low-pass filter, the fact that the magnitude of the notch filter is 0 at its characteristic frequency f_0 can provide local phase compensation for the MMC. In addition, the notch filter has a lesser impact on the control system than the low-pass filter.

The transfer function of a typical second-order notch filter is given by (6).

$$G_{\mathrm{f}}^{\mathrm{v}}(s) = \frac{s^2 + \omega_0^2}{s^2 + 2\xi\omega_0 s + \omega_0^2} \tag{6}$$

The denominator of (1) with a notch filter can also be expressed as (4), where θ_{f} is the phase of the notch filter.

The damping ratio ξ reflects the bandwidth of the notch filter. Near the characteristic frequency, the larger the value of ξ, the greater the positive phase compensation caused by the notch filter. However, before the characteristic frequency, the larger the value of ξ, the smaller the value of θ_{f} at the same frequency; correspondingly, the greater the negative phase compensation caused by the notch filter, the lower the frequency range of negative damping, and the higher the risk of the resonance frequency shift. The Bode plot of the denominator of (1) with a notch filter is exhibited in Fig. 7. In addition, in the actual system, there is usually more than one potential resonance point. Therefore, it's hard to suppress the high-frequency resonance by the addition of a single notch filter to the voltage feed-forward stage.

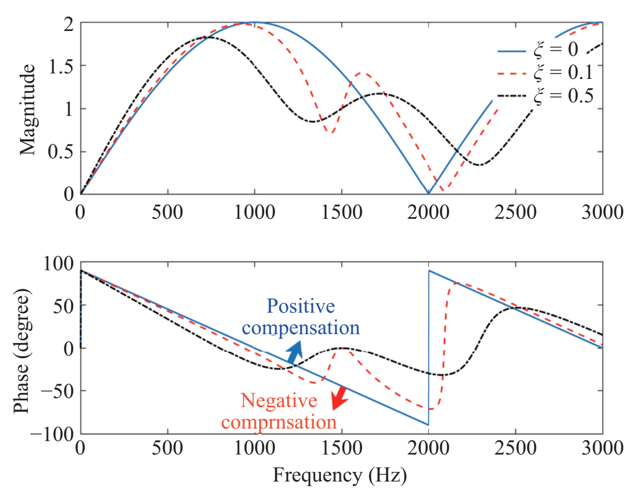

Fig. 7. Bode plot of the denominator of (1) with different values of ξ ($f_0 =$ 1500 Hz).

In this paper, a strategy of adding cascaded notch filters, as shown in Fig. 8, is proposed to suppress the high-frequency resonance of the MMC-HVDC system.

Each notch filter of the proposed strategy is for a different resonance point. And, the damping ratio of each notch filter can be set small to reduce the filter's impact on system stability, but should be large enough to provide enough phase

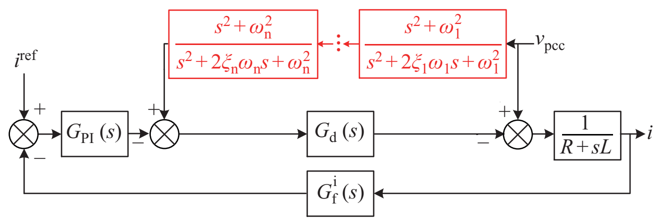

Fig. 8. The proposed additional damping control strategy block diagram.

compensation for the resonance point. Finally, the effect of the proposed strategy is to make all resonance points of the system obtain local compensation.

2) Parameters design

A large number of tests and simulations will be carried out before an actual project is put into operation, so the link delay and high-frequency characteristics can be basically obtained through the preliminary study. On this basis, the parameters design method of the proposed strategy is discussed.

1) Characteristic frequency

Since the notch filter may cause the resonance frequency to shift to a lower frequency, the parameters of the next notch filter need to be designed according to the parameters of the upper one.

For convenience, the characteristic frequency of the new notch filter is set to an integral multiple frequency of the fundamental frequency and near the current resonance point. It is possible that there are multiple resonance points in the system at the same time. At this time, the highest resonance point should be compensated first, because the negative compensation appears on the left of the characteristic frequency, which will change the impedance characteristics at the lower frequency. Therefore, the characteristic frequencies of the cascaded notch filters have the relation: $f_1 > f_2 > \cdots > f_n$.

1) Damping ratio

The relationships between the upper cut-off frequency f_U, the lower cut-off frequency f_L and the damping ration ξ, the characteristic frequency f_0 of a notch filter is given by (7).

$$\begin{cases} f_U = f_0 \times \left(\sqrt{\xi^2+1}+\xi\right) \\ f_L = f_0 \times \left(\sqrt{\xi^2+1}-\xi\right) \end{cases} \quad (7)$$

When a notch filter is set effectively, the resonance is eliminated or the resonance frequency shifts to a lower frequency. Therefore, on the left of the characteristic frequency, the frequency range of positive compensation caused by the notch filter should be at least 50 Hz, that is, $f_0 - f_L \geq 50$ Hz.

Since the damping ratio of the proposed strategy is small, f_U and f_L are approximately symmetric with respect to f_0, the relationship between ξ and f_0 is as follows:

$$\xi_{\min} = \frac{50}{f_0} \quad (8)$$

First, the damping ratio ξ of the notch filter is set to $\xi_{\min}$. When $\xi_{\min}$ cannot provide enough positive phase compensation for the resonance point, it is necessary to increase ξ.

The parameters design process of the cascaded notch filters is shown in Fig. 9.

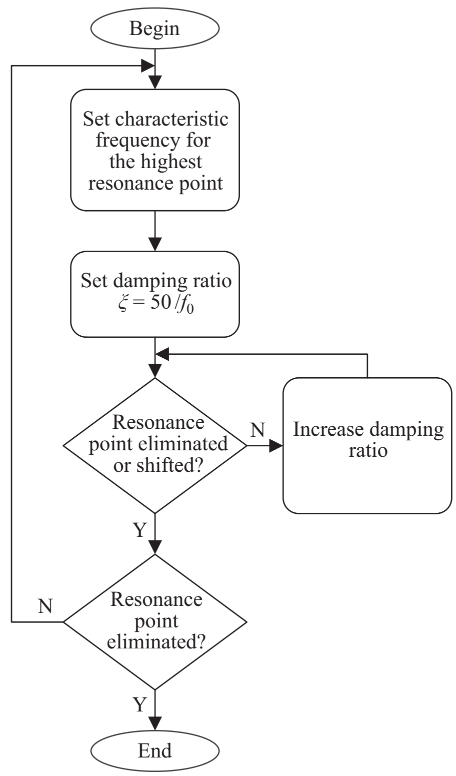

Fig. 9. Parameters design process of the cascaded notch filters.

It should be noted that, although the additional cascaded notch filters can reduce the influence on the control system of the MMC as compared to the low-pass filter, the parameters should be re-determined when the system resonance changes due to the change of the operating conditions.

C. Additional Damping Control for Other Structures

$G_{add}(s)$ represents the transfer function of the additional control. The position of $G_{add}(s)$ in the inner controller of the MMC roughly has four situations, as shown in Fig. 10.

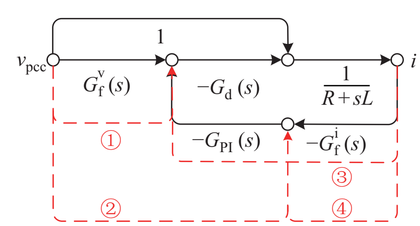

Fig. 10. Signal flow graph of other additional damping control strategies.

The expression of $Z_M(s)$ of each structure is given by (9).

$$\begin{cases} Z_M(s) = \frac{R+sL+G_f^i(s)G_d(s)G_{PI}(s)}{1-[G_f^v(s)+G_{add}(s)]G_d(s)} \\ Z_M(s) = \frac{R+sL+G_f^i(s)G_d(s)G_{PI}(s)}{1-[G_f^v(s)-G_{add}(s)G_{PI}(s)]G_d(s)} \\ Z_M(s) = \frac{R+sL+[G_f^i(s)G_{PI}(s)+G_{add}(s)]G_d(s)}{1-G_f^v(s)G_d(s)} \\ Z_M(s) = \frac{R+sL+[G_f^i(s)-G_{add}(s)]G_d(s)G_{PI}(s)}{1-G_f^v(s)G_d(s)} \end{cases} \quad (9)$$

It is evident that the effect of $G_{add}(s)$ is similar to the effects of $G_f^v(s)$ and $G_f^i(s)$. The additional control applied to the current acts on the numerator of (9), and the influence on the high-frequency impedance characteristics of the MMC is masked by L. The additional control applied to the voltage acts on the denominator, and the effect is the same as that of the feed-forward voltage filter, as are the disadvantages.

D. The Limitations of Additional Damping Control Strategies

From the preceding analysis of the mechanisms of various additional damping control strategies, it is evident that the filter can indeed play a phase-compensation role, but it cannot improve the damping of the MMC in the entire high-frequency range, which is likely to cause the shift of the resonance frequency. By comparison, the strategy of including an additional low-pass filter has stronger adaptability, and the strategy of including additional cascaded notch filters has less influence on the response of the controller; however, both strategies require accurate models and numerous simulation tests to design parameters in engineering practice.

IV. Simulation Results

A. The High-frequency Resonance Phenomenon

In the simulated system of the northern route of the Chongqing-Hubei project, under the normal operating conditions, the link delay of 500 μs will not cause high-frequency resonance. Fig. 11(b) presents the time-domain simulation of the phase-A voltage at the PCC. Fig. 11(a) exhibits the impedance-frequency characteristics of the system obtained by the frequency scanning method. It is evident that the impedance-frequency curve of the MMC is approximately consistent with that in Fig. 3, and the phase margin of each potential resonance point is within the safe range.

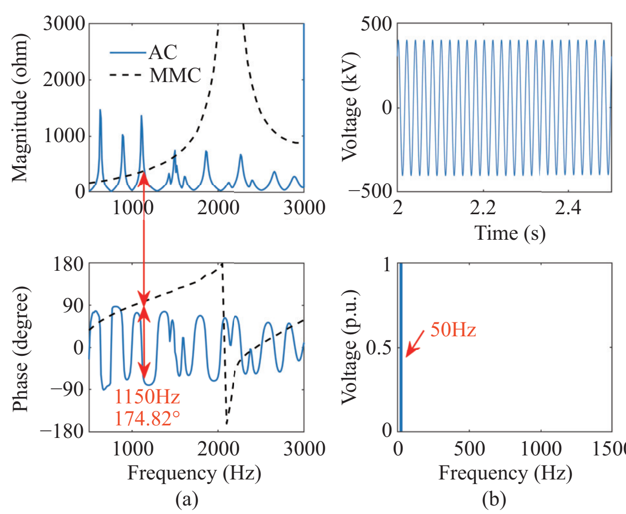

Fig. 11. Impedance analysis and time-domain simulation of normal operating conditions. (a) The impedance characteristics determined by the frequency scanning method; (b) The time-domain simulation of the PCC.

When one of the overhead lines at the PCC is disconnected, the high-frequency impedance characteristics of the AC system change, and severe high-frequency resonance occurs in the system. As shown in Fig. 12(b), the disconnection fault of the AC system occurs at $t = 2.6$ s, and the main resonance frequency of the fault system is 1650 Hz. It can also be seen from the impedance-frequency curves shown in Fig. 12(a) that the phase deviation of the fault system at 1660 Hz has exceeded the safe range.

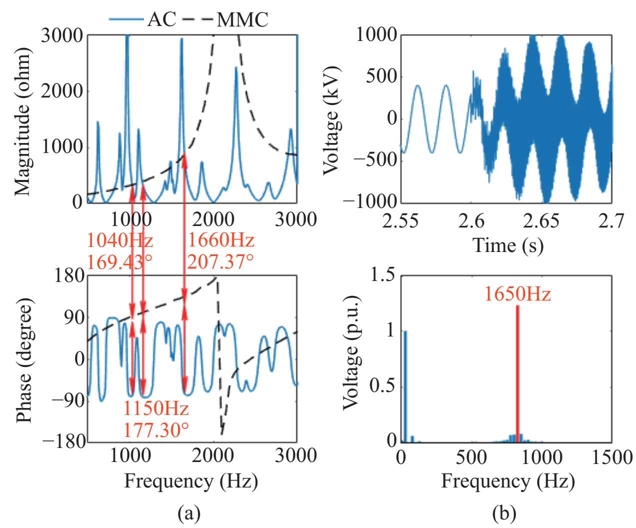

Fig. 12. Impedance analysis and time-domain simulation of the fault operating condition. (a) The impedance characteristics determined by the frequency scanning method; (b) The time-domain simulation of the PCC.

B. Verification of the Effectiveness and Limitations of Additional Damping Control Strategies

1) Additional Feed-forward Voltage Low-pass Filter

In this study, the first-order low-pass filter is selected for verification. Fig. 13 presents the impedance-frequency curves of the system after adding low-pass filters with different cut-off frequencies.

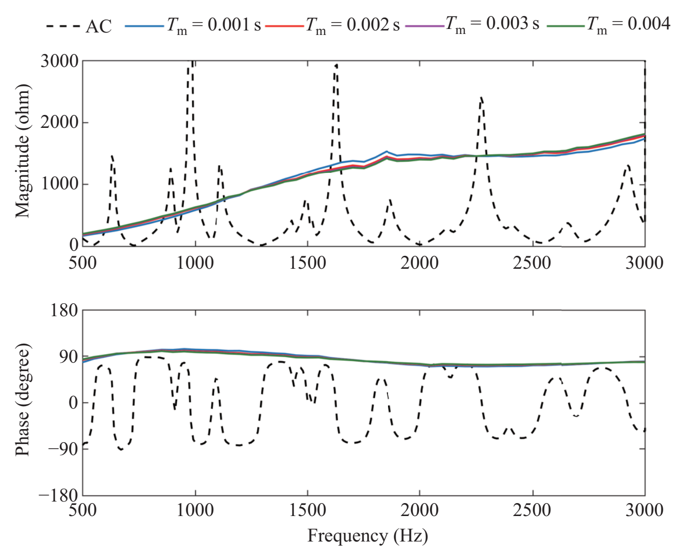

Fig. 13. Impedance analysis after adding a low-pass filter.

The low-pass filter causes the frequency range of the negative damping of the MMC to shift. If the cut-off frequency is not small enough, the phase deviation at the potential resonance point still exceeds the safe range, as shown in Table II.

When $T_m = 0.004$ s, the phase margins of all potential

TABLE II
SYSTEM RESONANCE AFTER ADDING A LOW-PASS FILTER

Time Constant $T_{\rm m}$	Resonance Frequency	Phase Deviation
0.001 s	1020 Hz	182.49°
0.002 s	660 Hz	181.46°
0.003 s	660 Hz	180.26°

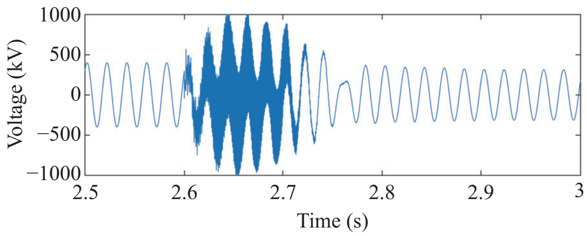

Fig. 14. The time-domain simulation of the PCC after adding a low-pass filter ($T_{\rm m}$ = 0.004 s).

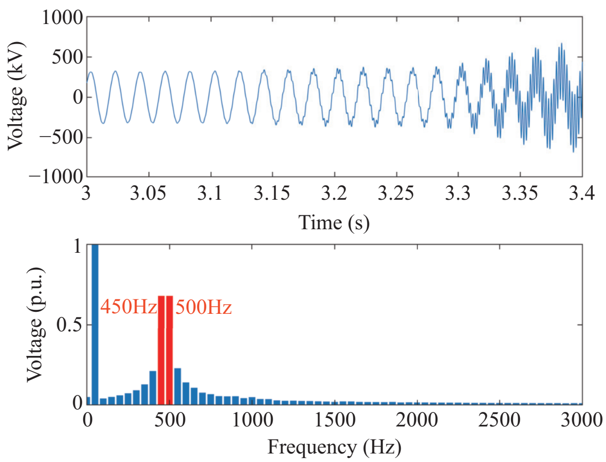

Fig. 15. The time-domain simulation of the PCC after adding a low-pass filter ($T_{\rm d}$ = 630 μs, $T_{\rm m}$ = 0.004 s).

resonance points are within the safe range. After the low-pass filter is applied to the fault system at $t = 2.7$ s, the resonance is quickly suppressed, as shown in Fig. 14.

However, the compensation effect of the low-pass filter is limited. When the link delay is increased from 500 μs to 630 μs at $t = 3$ s under the fault condition, the low-pass filter with $T_{\rm m} = 0.004$ s can no longer suppress the resonance, and the simulation result is exhibited in Fig. 15.

2) Additional Feed-forward Voltage Cascaded Notch Filters

Because the resonance frequency of the fault system is 1650 Hz, a single notch filter with a characteristic frequency of 1650 Hz and the respective damping ratios of 0.01, 0.03, and 0.1 is added. The impedance characteristics of the fault system after adding the single notch filter are shown in Fig. 16.

It is evident that a too small damping ratio cannot provide enough phase compensation, but a larger damping ratio will shift the resonance frequency of the system. As exhibited in Table III, with the increase of the damping ratio, the resonance frequency shifts to a lower frequency, which is consistent with the aforementioned mechanism analysis. This proves that the high-frequency resonance of the MMC-HVDC system cannot be suppressed by adding a single notch filter.

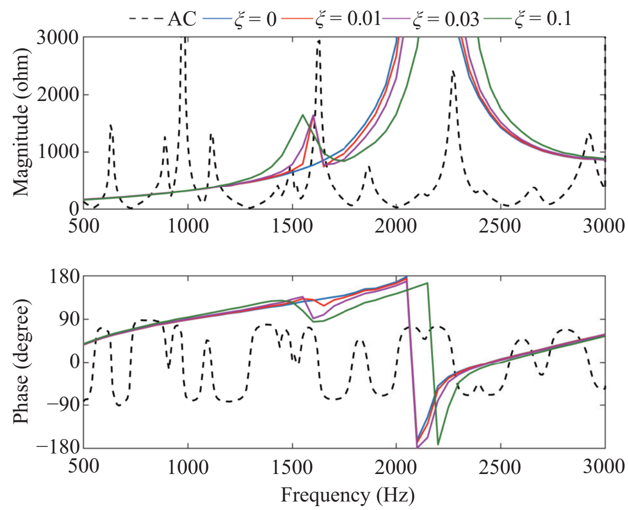

Fig. 16. Impedance analysis after adding a single notch filter.

TABLE III
SYSTEM RESONANCE AFTER ADDING A SINGLE NOTCH FILTER

Damping Ratio ξ	Resonance Frequency	Phase Deviation
0.01	1660 Hz	194.31°
0.03	1160 Hz	181.74°
0.1	1150 Hz	185.24°

TABLE IV
THE PARAMETERS OF CASCADED NOTCH FILTERS

Characteristic Frequency f_0	Damping Ratio ξ
1650 Hz	0.03
1150 Hz	0.043
1050 Hz	0.048
1000 Hz	0.05

The proposed strategy of the inclusion of additional cascaded notch filters is adopted, and the parameters are set according to the proposed parameters design method, as shown in Table IV.

The impedance-frequency curves of the fault system after adding the cascaded notch filters are shown in Fig. 17(a), in which the phase deviation of each potential resonance point is less than 180°. The time-domain simulation of the phase-A voltage at the PCC is exhibited in Fig. 17(b). After the additional control is put into operation at $t = 2.7$ s, the high-frequency resonance is quickly suppressed, and the suppression effect is consistent with that shown in Fig. 14.

However, when the link delay changes greatly or the AC system topology changes, resulting in the change of the system resonance point, the parameters of the cascaded notch filters should be reset. As shown in Fig. 18, when the link delay increases from 500 to 600 μs at $t = 3$ s, the previous parameters cannot provide enough phase compensation near 1000 Hz.

C. Influence of Additional Damping Control Strategies on the Control System

Under the link delay $T_{\rm d}$ = 500 μs and the disconnection fault of the AC system, the DC voltage command is set to decrease from 1 to 0.95 p.u. at $t = 4$ s, and to increase from

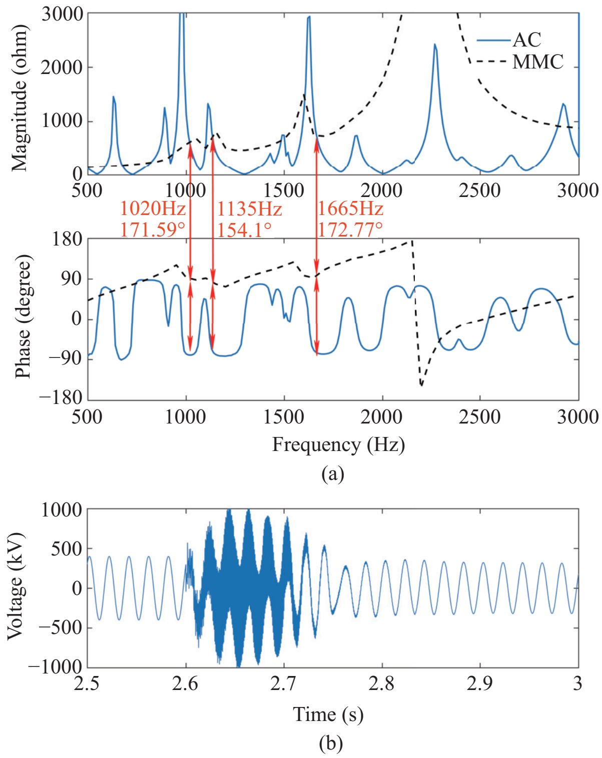

Fig. 17. Impedance analysis and time-domain simulation after adding cascaded notch filters. (a) The impedance characteristics determined by the frequency scanning method; (b) The time-domain simulation of the PCC.

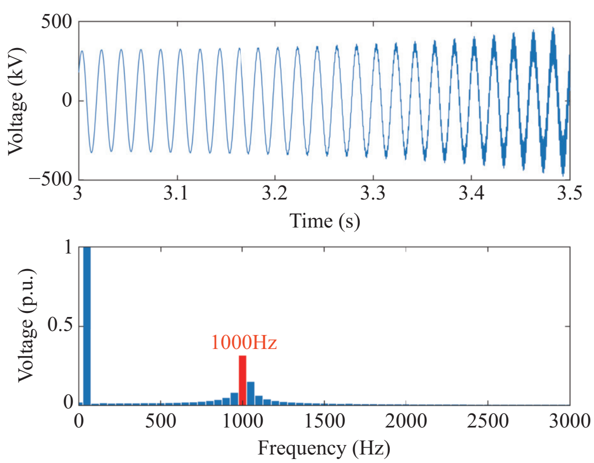

Fig. 18. The time-domain simulation of the PCC after adding cascaded notch filters ($T_{\mathrm{d}} = 600$ μs).

0.95 to 1 p.u. at $t = 4.5$ s. Fig. 19 presents the responses of the system with different additional control strategies as compared to those of the system with no link delay and no additional control.

Because the low-pass filter reduces the components of the feed-forward voltage in a wide frequency range, the ability of the controller to respond to the dynamic change is weakened. In contrast, the response ability of the controller with cascaded notch filters is closer to that of the original system.

V. Conclusion

In this paper, additional damping control strategies for the suppression of the high-frequency resonance of the MMC-HVDC system were analyzed in detail. Additionally, a strategy of the inclusion of additional cascaded notch filters was proposed in combination with engineering practice, and the limitations of the existing and proposed strategies were theoretically analyzed. The following conclusions are obtained:

1) In the inner controller of the MMC, the influence of the voltage feed-forward stage on the high-frequency impedance characteristics of the MMC is greater than that of the current feed-back stage;

2) The order of additional low-pass filters of the feed-forward voltage have little influence on the resonance suppression effect. Reducing the cut-off frequency is the most effective method by which to improve the resonance suppression effect, but has a great impact on the controller's performance. Therefore, this strategy is suitable for situations with low transient performance requirements;

3) As compared to a single notch filter, cascaded notch filters can achieve the phase compensation of all resonance points of the system. This strategy can effectively reduce the impact on the controller's performance while suppressing the resonance, but cannot adapt to a large change in the impedance characteristics of the system. Therefore, it is suitable for situations in which the structure of the AC system is relatively fixed and the link delay of the DC system has a small range of variation;

4) At present, the additional damping control strategies for the high-frequency resonance of the MMC-HVDC system cannot take into account both the adaptability and controller's performance, and when the parameters are not set properly, the resonance frequency will shift. In further research, the combination of fast frequency detection technology and cascaded notch filters should be considered to improve the application scope of the proposed strategy.

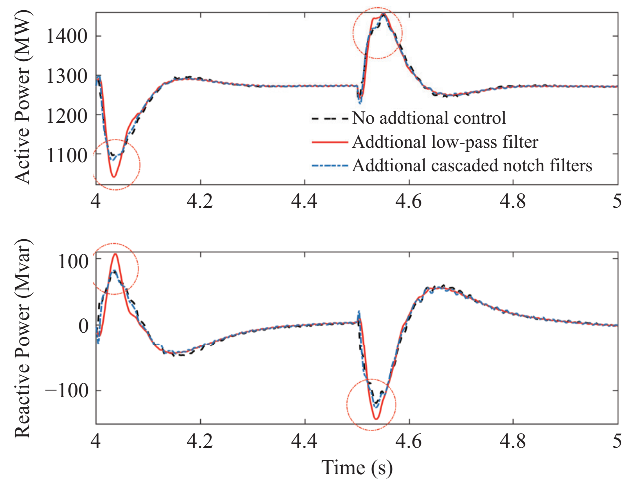

Fig. 19. Response of the MMC.

References

[1] A. Lesnicar and R. Marquardt, "An innovative modular multilevel converter topology suitable for a wide power range," in *Proceedings of 2003 IEEE Bologna Power Tech Conference*, Bologna, Italy, 2003, pp. 23–26.

[2] A. Dekka, B. Wu, R. L. Fuentes, M. Perez, and N. R. Zargari, "Evolution of topologies, modeling, control schemes, and applications of modular multilevel converters," *IEEE Journal of Emerging and Selected Topics in Power Electronics*, vol. 5, no. 4, pp. 1631–1656, Dec. 2017.

[3] T. H. Nguyen, K. Al Hosani, M. S. El Moursi, and F. Blaabjerg, "An overview of modular multilevel converters in HVDC transmission systems with STATCOM operation during pole-to-pole dc short circuits," *IEEE Transactions on Power Electronics*, vol. 34, no. 5, pp. 4137–4160, May 2019.

[4] Y. Hu, J. Chen, C. Y. Zou, J. Y. Zhou, and W. X. Lin, "Experimental investigation on communication link delay of valve control system of ultrahigh-voltage VSC-HVDC," *Journal of Global Energy Interconnection*, vol. 3, no. 2, pp. 190–198, Mar. 2020.

[5] C. Y. Zou, B. Y. Liu, S. X. Duan, and R. Li, "Influence of delay on system stability and its optimization in grid-connected inverters," *Proceedings of the CSEE*, vol. 35, no. 2, pp. 411–417, Jan. 2015.

[6] X. T. Zhang, J. W. Spencer, and J. M. Guerrero, "Small-signal modeling of digitally controlled grid-connected inverters with LCL filters," *IEEE Transactions on Industrial Electronics*, vol. 60, no. 9, pp. 3752–3765, Sep. 2013.

[7] C. Buchhagen, C. Rauscher, A. Menze, and J. Jung, "BorWin1-First experiences with harmonic interactions in converter dominated grids," in *Proceedings of International ETG Congress 2015; Die Energiewende - Blueprints for the New Energy Age*, Bonn, Germany, 2015, pp. 1–7.

[8] C. Q. Yin, X. R. Xie, H. Liu, X. Wang, Z. B. Wang, and Y. N. Chi, "Analysis and control of the oscillation phenomenon in VSC-HVDC transmission system," *Power System Technology*, vol. 42, no. 4, pp. 1117–1123, Apr. 2018.

[9] Y. Li, C. Y. Zou, H. Rao, S. K. Xu, C. Hong, L. B. Huang, and W. W. Li, "Resonance of VSC-HVDC with extreme AC grid," *Proceedings of the CSEE*, vol. 38, no. S1, pp. 19–23, Aug. 2018.

[10] Q. Guo, H. P. Guo, and L. B. Huang, "Effect of grid voltage feedforward on VSC-HVDC stability in weak power grid," *Automation of Electric Power Systems*, vol. 42, no. 14, pp. 139–144, Jul. 2018.

[11] Z. W. Xie, Y. D. Chen, W. H. Wu, X. Y. Wang, and Z. L. Wang, "A global high-frequency oscillation suppression method for multi-Inverter grid-connected system in weak grid," *Transactions of China Electrotechnical Society*, vol. 35, no. 4, pp. 885–895, Feb. 2020.

[12] J. M. Liu, Y. D. Chen, W. H. Wu, K. Zhang, and A. Luo, "Sequence impedance modeling and high-frequency oscillation suppression method for island microgrid," *Transactions of China Electrotechnical Society*, vol. 35, no. 7, pp. 1538–1552, Apr. 2020.

[13] C. Y. Zou, H. Rao, S. K. Xu, Y. Li, W. W. Li, J. Chen, X. B. Zhao, Y. Yang, and B. Lei, "Analysis of resonance between a VSC-HVDC converter and the AC grid," *IEEE Transactions on Power Electronics*, vol. 33, no. 12, pp. 10157–10168, Dec. 2018.

[14] X. S. Guo, B. Liu, H. M. Mei, J. Liu, H. L. Yu, and F. M. Cao, "Analysis and suppression of resonance between AC and DC systems in Chongqing-Hubei back-to-back HVDC project of China," *Automation of Electric Power Systems*, vol. 44, no. 20, pp. 157–164, Oct. 2020.

[15] X. S. Guo, Z. H. Liu, Y. F. Li, and Y. J. Lu, "Characteristic analysis of high-frequency resonance of flexible high voltage direct current and research on its damping control strategy," *Proceedings of the CSEE*, vol. 40, no. 1, pp. 19–29, Jan. 2020.

[16] D. Y. Du, C. Y. Guo, X. F. Jia, C. Y. Zhao, and Y. H. Hu, "Suppression strategy for high frequency resonance of modular multilevel converter based on additional band-stop filter," *Transactions of China Electrotechnical Society*, vol. 36, no. 7, pp. 1516–1525, Apr. 2021, doi: 10.19595/j.cnki.1000–6753.tces.200077.

[17] H. Saad, Y. Fillion, S. Deschanvres, Y. Vernay, and S. Dennetière, "On resonances and harmonics in HVDC-MMC station connected to AC grid," *IEEE Transactions on Power Delivery*, vol. 32, no. 3, pp. 1565–1573, Jun. 2017.

Yanqi Hou received a B.S. degree in Electrical Engineering and Automation from the School of Electrical and Electronic Engineering, North China Electric Power University, Beijing, China, in 2018. He is currently pursuing a Ph.D. degree in Electrical Engineering at the School of Electrical and Electronic Engineering, North China Electric Power University, Beijing, China. His research interests include modeling and control of flexible HVDC transmission systems.

Chongru Liu (M'10–SM'15) received B.S., M.S., and Ph.D. degrees in Electrical Engineering from Tsinghua University, Beijing, China. She was a Visiting Professor with The University of Hong Kong, from 2009 to 2010, and a Visiting Professor with Washington State University, from 2010 to 2011. She is currently a Professor with the School of Electrical and Electronic Engineering, North China Electric Power University. She is a member of the National Power System Management and Information Exchange Standardization Committee of China. She is also a member of Beijing Nova and supported by the program of New Century Excellent Talents in University.

Yu Wang received the B.S. and Ph.D. degrees in Electrical Engineering from North China Electric Power University, Beijing, China. He was a visiting Ph.D. student with University of Toronto from 2019 to 2020. He is currently an Electrical Engineer with State Grid Economic and Technological Research Institute Co. Ltd., Beijing, China. His main research interests include design and control of HVDC transmission systems.

Wei Kong received the Ph.D. degree from North China Electric Power University, Beijing. He is currently an Electrical Engineer with State Grid Corporation of China, Beijing, China. His main research interests include design and control of HVDC transmission systems.